Journal of Alloys and Metallurgical Systems 9 (2025) 100139

Contents lists available at ScienceDirect

Journal of Alloys and Metallurgical Systems

journal homepage: www.journals.elsevier.com/journal-of-alloys-and-metallurgical-systems

An *ab-initio*, empirical and experimental study of phase stability of HfTiVYZr refractory high entropy alloy

Vivek Kumar Pandey [a,b,*], B. Nageswara Sarma [a], N.K. Mukhopadhyay [a]

[a] Department of Metallurgical Engineering, Indian Institute of Technology (Banaras Hindu University), Varanasi 221005, India
[b] Department of Mechanical Engineering, School of Engineering, Presidency University, Bangalore 560064, India

ARTICLE INFO

Keywords:
High Entropy Alloy
CALPHAD
Density Functional Theory
Vaccum Arc Melting
Characterization

ABSTRACT

Phase evolution and stability in an equiatomic quinary HfTiVYZr refractory high entropy alloy (RHEA) was studied. Prediction of phases that may form on the synthesis of the above alloy was made by using (i) Semi-empirical/empirical methods (based on extended Hume-Rothery rules), (ii) CALPHAD and (iii) *ab-initio* methods. Enthalpy of mixing of HfTiVYZr high entropy alloy calculated using the Miedema model ($\Delta H_{mix} = 7$ kJ. mol^{-1}) was close to the proposed range favouring the formation of single-phase solid solution ($-10 \leq \Delta H_{mix} \leq 7 kJ.mol^{-1}$). However, the size mismatch factor δ(10.37 %) was unfavourable for forming the single-phase solid solution. As per the prediction of the CALPHAD approach, three disordered HCP solid solutions and one C15 type Laves phase (ZrV_2) were found to be stable at room temperature, whereas the ordered BCC_B2 phase was identified to be stable above 1273 K. The DFT approach using a variation of the cluster expansion method with fixed composition and cell size was adopted to study the phase stability of this refractory alloy. Enthalpies of mixing of BCC and HCP structures were calculated for the distinct configuration of atoms on the atomic sites using a ten-atom cell. The annealed alloy was examined by XRD, SEM and SEM-EDS. The annealed sample shows the presence of two disordered HCP phases, namely, HCP1 ($a = 3.18 \pm 0.02$ Å, $c/a = 1.58$) and HCP2 ($a = 3.67 \pm 0.02$ Å, $c/a = 1.55$), along with a BCC phase ($a = 3.16 \pm 0.02$ Å) and an ordered intermetallic phase (Hf, Zr)V_2 (C15 type Laves phase, $a = 7.41 \pm 0.02$ Å), which is in accordance with the theoretical predictions. The SEM-EDS mapping of the annealed sample shows that the major HCP1 phase contains Hf and Zr predominantly along with some Ti.

1. Introduction

High Entropy Alloys (HEAs) [1,2], Multi-Principal Element Alloys (MPEAs) [3] and Complex Concentrated Alloys (CCAs) [4] signify a similar alloying concept. The multi-principal alloying concept explores the otherwise unexplored central region of the multicomponent phase diagrams. In the initial stages of the development of HEAs, it was conjectured that one would easily obtain solid solutions due to higher configurational entropy. However, later work has shown that various other factors such as enthalpy of mixing, atomic radius ratio and valence electron concentration also control the formation of simple solid solutions. A limited number of single-phase HEAs are reported to date. Gao et al. [5] have proposed combining the phase diagram and *ab-initio* methods to strengthen the search for single-phase HEAs. They suggested that forming isomorphous solid solutions in the binary and ternary subsystems would lead to single-phase HEAs in the higher component systems.

The refractory high entropy alloys (RHEAs) were first reported in 2010 by Senkov *et al.* [6] as two equiatomic MoNbTaW and MoNbTaVW quaternary and quinary alloys based on the refractory elements (Mo, Nb, Ta, V, W). Both the alloys exhibited a single-phase BCC structure and showed exceptional strength (~400 MPa) at 1873 K. Senkov et al. [7] reported a single BCC phase in the equiatomic HfNbTaTiZr quinary HEA synthesized by vacuum arc melting. Gao et al. [5] have studied HfNbTaTiVZr by adding vanadium to the single-phase BCC forming an equiatomic HfNbTaTiZr quinary system. They have checked the senary system by inspecting binary and ternary phase diagrams and using enthalpy of mixing for binary compounds found from density functional theory (DFT). Pandey et al. [8] have obtained two BCC phases along with minor amounts of ordered B2 and C15 type Laves phases co-existing in the as-cast sample in MoTiVWZr RHEA. The primary BCC phase (BCC#1) is rich in Mo and W ($a = 3.17 \pm 0.02$ Å), while the

* Corresponding author at: Department of Mechanical Engineering, School of Engineering, Presidency University, Bangalore 560064, India.
E-mail address: vivek.rs.met13@itbhu.ac.in (V.K. Pandey).

https://doi.org/10.1016/j.jalmes.2024.100139
Received 16 September 2024; Received in revised form 2 December 2024; Accepted 4 December 2024
Available online 9 December 2024

minor BCC phase (BCC#2) is rich in Zr and Ti ($a = 3.65 \pm 0.02$ Å). The annealed sample shows a transformation of the disordered BCC phases to the ordered B2 phases and an increase in the C15 Laves phase.

Most of the solid solution phases reported in HEAs have either BCC or FCC structures [9–12]. The HEAs exhibiting single-phase HCP structures are limited in number, a few examples of which are: DyGdLuTbY [13], DyGdLuTbTm [13], DyHoGdTbY [14], HfLaScTiYZr [15] and AlHfScTiZr [16]. Nagase et al. [17] have used the concept of liquid phase separation to design a structure having two HCP phases in HfLaTiYZr using mixing enthalpy data for the binary subsystems and phase diagrams constructed using Materials Project. They obtained Ti-Zr-Hf rich dendritic phase and Y-La rich inter-dendritic phase in the as-cast ingot. Fazakas et al. [18] fabricated TiZrHfNbV and TiZrHfNbCr RHEAs using induction melting route. It is important to note that TiZrHfNbV alloy formed a single BCC phase, whereas TiZrHfNbCr exhibited BCC as the major phase co-existing with a small amount of $NbCr_2$ and $HfCr_2$ cubic (C15) Laves phases. The structural and mechanical properties remained unchanged up to 1173 K.

It can be seen that Ti, Zr and Hf are common elements among the above-reported RHEAs exhibiting HCP and BCC phases. If Co, Cr, Mo, Nb and Ta are added to Ti-Zr-Hf, then the HEAs can also be designed for biomedical applications. Nagase et al. [19] have developed CrHfMoTiZr and CoCrMoHfTiZr as metallic biomaterials, which are claimed to have better hardness and biocompatibility than the Ti-based alloys that are currently being used for surgical implants. Calin et al. [20] have developed HfNbSiTiZr HEA as a magnetic resonance imaging compatible metallic glass. This glassy alloy has ultralow magnetic susceptibility and a superior X-ray attenuation coefficient.

Huang et al. [21] prepared three refractory alloys based on HfTiZr, viz., HfScTiZr, HfTiYZr and HfScTiYZr HEAs. The addition of Sc to a single HCP structured HfTiZr alloy resulted in a dual HCP structure, having improved strength and ductility. While adding Y to the HfTiZr alloy resulted in two HCP phases. The primary HCP phase is disordered with a small amount of undissolved Y (HCP2). Adding Sc and Y to HfTiZr alloy resulted in a dual HCP phase and a small amount of undissolved Y.

The DFT is used to solve complex many-particle Schrödinger equation; it acts as a powerful tool for predicting the formation of phases (e.g., BCC, FCC and HCP) and their stability under different conditions. The stability of these various phases is determined by the relative energy of specific atomic arrangement on a given lattice type that can change with concentration. The disordered solid solution cell can be designed mainly by coherent potential approximation (CPA) [22], special quasirandom structure (SQS) [23] and cluster expansion method [24]. The cluster expansion method [24–27], has been widely used to study the mixing of two (or more) atoms in an alloy phase with a given lattice symmetry by changing the concentration of different atom types for computing the relative energy by DFT calculation. Thus, we focus on the total energy (or relative energy) on replacement of these sites' occupation with the different chemical species. Some most commonly used codes to build cluster expansion are the Universal Cluster Expansion Code (UNCLE) [26], Alloy Theoretic Automated Toolkit (ATAT) [28], and CLUPAN [29].

Mu et al. [30] studied MoTiVZr, MoTaTiVZr, MoNbTaTiVZr, CrMoNbTaTiVZr and CrMoNbTaTiVWZr alloy systems by employing the *ab-initio* method to estimate formation enthalpy and cohesive energy to examine the stability of the above refractory alloys. They have calculated the theoretical elastic constants and bulk modulus for alloy systems, which exhibit variation in mechanical anisotropy.

In the present study, we aim to study the phase stability of the HCP phase by adding vanadium to previously studied HfTiYZr HEA. The HfTiYZr alloy is forming a single-phase HCP solid solution along with a small amount of undissolved Y. A theoretical and experimental investigation of HfTiVYZr RHEA is carried out in the present study to understand the evolution of phases and their stability. Since the C15 Laves phase is very stable in Hf-V and Zr-V binary systems, it will be interesting to explore the effect of V addition on the HfTiYZr HEA as the likelihood of Laves phase formation increases.

2. Computational method

Initially, the phases that may form in the chosen alloy system were predicted by using semi-empirical Miedema's model [31] and by calculating binary phase diagrams for subsystems. The enthalpy values of binary subsystems were extrapolated for the quinary system, using the regular solution model. The other parameters that affect the stability of the alloy, i.e., the entropy of mixing (ΔS_{mix}), atomic size mismatch (δ) [32] and valence electron concentration (VEC) [33] were calculated using the weighted average method.

In materials, there are various phases defined by an underlying spatial lattice (e.g., BCC, FCC for many metals and alloys). The stability of these phases is determined by the relative energy of the specific arrangement of the individual atoms on a given lattice type, which also can change with concentration. In the cluster expansion method, because the underlying spatial lattice type remains largely constant around the original positions of the nuclear coordinates ($R_1 \ldots\ldots R_m$), we can focus on what happens to the total energy (or relative energy) if we replace some atoms of a given species with another atom species for the set of known atomic positions in the crystal. In this case, the energy (E) becomes a simple function of the occupation of these sites by the different chemical species (Z):

$$E(R_1, \ldots\ldots, R_m) = E_{conf}(Z_1, \ldots\ldots, Z_m) \quad (1)$$

The cluster expansion method has been used by choosing a cell with fixed composition and lattice sites. A 10-atom primitive cell of BCC and HCP was chosen and 5 elements were distributed over 10 sites. The total number of ways of arranging 5 elements over 10 atomic sites is equal to 1,13,400. A total of 22,680 structures were obtained by removing the equivalent structures from the list. In a 10-atom BCC primitive cell, we have considered pairs (up to 3rd neighbour distances) and triangle interactions to obtain distinct structures. Thus, the number of distinct working configurations was reduced to 5925. For the 10 atom cell in HCP, we have considered pair interactions only up to 3rd neighbour distances which resulted in a total of 11,040 distinct structures. Representative cells in the case of BCC and HCP structures are shown in Figs. 1 and 2 respectively.

We have used Quantum Espresso software (version 6.4) for performing the first principles calculations. Before starting the calculations for the alloy systems, we have optimized the values of energy cut-off (E_{cut}), k-points and the lattice parameters of the individual elements. The energy cut-off of the calculations is fixed by converging the total energy of the elements with respect to increasing E_{cut} value. Similarly, the k-points samplings must be tested with respect to energy

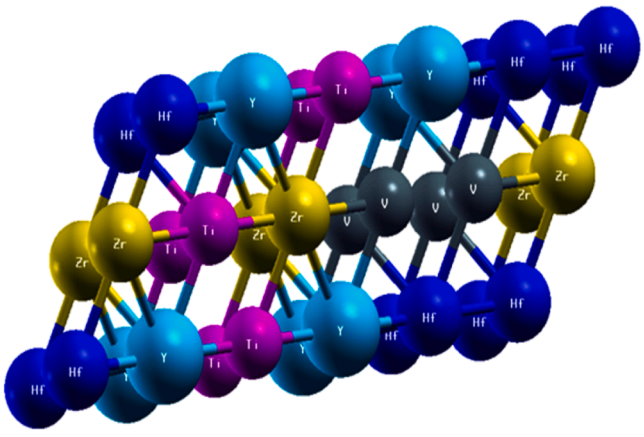

Fig. 1. : A representative structure of 10 atom primitive BCC cell over which 5 elements are distributed.

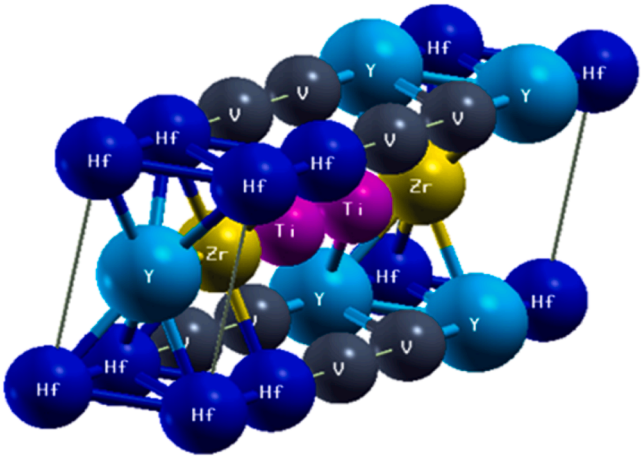

Fig. 2. : A representative structure of 10 atom primitive HCP cell over which 5 elements are distributed.

convergence. The optimization of the energy cut-off and k-points needs to be carried out because accuracy improves with increasing values of these parameters but the computational burden in terms of calculation time increases exponentially. The optimized values of E_{cut} and k-points used in the calculations of the energies of HfTiVYZr are 45 Ry and 10x10x10 (in x, y, and z directions), respectively. The details of optimization are presented in supplementary data attached.

3. Experimental techniques

We have taken elemental powders of Ti, V and Y from Alfa Aesar and those of Hf and Zr from Otto Chemie Pvt. Ltd. having purity above 99.9 % and mechanically mixed them. The mechanical mixture of the elemental powders was compressed using a hydraulic press under a 2-tonne load to obtain a compressed pellet (10 mm diameter and 20 mm height), which was melted in a vacuum arc furnace in an argon atmosphere. Before melting the actual compacted powder, an electric arc was struck on a small piece of Ti to ensure absorption of any oxygen present in the chamber. The alloy button thus prepared was re-melted five times to ensure proper mixing of the elements. The button has a diameter of 22 mm and a thickness of 5 mm. The button was cut into half using a slow-speed precision cutter. The as-cast sample was annealed for 7 h, and furnace-cooled to obtain equilibrium phases in the chosen alloy system. The morphology of the annealed sample was examined using a scanning electron microscope (FEI Quanta 200 F 20 kV) operated at 20 kV and equipped with an energy-dispersive X-ray spectrometer. The XRD analysis was carried out on a Rigaku Mini flex-600 (40 kV-15 mA) with Cu-K_α radiation to analyze the phases formed in the prepared sample.

4. Results

4.1. Phase prediction based on parametric and CALPHAD approaches

A few parameters were calculated based on the extended Hume-Rothery rules for solid solution forming. These consisted of (i) enthalpy of mixing (ΔH^{ij}_{mix}) for the binary subsystems using the Miedema model, (ii) weighted average of atomic size mismatch (δ) and (iii) valence electron concentration (VEC). The enthalpies of mixing values for the binary subsystems are shown in Table 1. It can be seen that Ti-Zr, Hf-Ti and Hf-Zr have good mutual solubility, whereas Ti-V, V-Zr and Hf-V have significant negative enthalpy indicating the formation of intermetallic phases. Y has a highly positive enthalpy of mixing with the other elements of the group, meaning that Y may be immiscible with other elements of the alloy. The enthalpy of mixing for the quinary alloy

Table 1
Enthalpy of mixing (in kJ.mol^{-1}) for all the binary sub-systems in TiVYZrHf HEA computed using Miedema model.

Elements	Ti	V	Y	Zr	Hf
Ti	-	−2	15	0	0
V	−2	-	17	−4	−2
Y	15	17	-	9	11
Zr	0	−4	9	-	0
Hf	0	−2	11	0	-

(ΔH_{mix}= 7 kJ mol^{-1}) was calculated by extrapolating the enthalpy of mixing of binary alloys using the regular solution model, as shown in Table 2. The atomic size mismatch parameter was calculated using the formula proposed by Fang [34]. This indicated severe lattice distortion that is experienced by the parent lattice in a multicomponent system. Zhang et al. [35] proposed that for the solid solution formation in any alloy, the δ parameter must be ≤ 6.6. Valence electron concentration (VEC) values represent the total number of electrons present in the valence band and help in deciding the type of phases (BCC or FCC) that may form. Guo et al. [33] reported that the formation of FCC phase was favourable for VEC ≥ 8, whereas single-phase BCC structure was expected for VEC ≤ 6.8. For intermediate values lying in between the specified range, a mechanical mixture of two phases (BCC+FCC) may form.

Phase diagrams of the ten binary subsystems belonging to the quinary RHEA have been calculated using Thermo-Calc software and SGTE binary solution database version 5. The results are presented in Fig. 3. It can be seen that Hf-Ti, Hf-Zr and Ti-Zr systems exhibit extended solubility in the disordered HCP as well as in the BCC phases, whereas Hf-Ti, Ti-V and V-Zr exhibit a small miscibility gap, resulting in a two-phase mixture. It can be seen that wide miscibility gaps are present in the Hf-Y, Ti-Y, V-Y, and Y-Zr phase diagrams as shown in Fig. 3. At room temperature two-phase mixture of disordered HCP1 and HCP2 is present in Ti-Y and Y-Zr phase diagrams, while BCC_B2 and disordered HCP phases are present in Hf-Y and V-Y phase diagrams. No other Laves phase except for ZrV_2 formed in the V-Zr phase diagram are present.

We have also collected phase diagrams from the Binary Alloy Phase Diagrams handbook [36], which are shown in Fig. 5. It may be noted that there are considerable differences in the Hf-V and Hf-Y phase diagrams calculated using Thermo-Calc software and those given in Massalski's handbook. The discrepancy in the computed binary phase diagrams of Hf-V and Hf-Y systems is due to the fact that the Thermo-Calc database used might not have been optimized for these systems.

The equilibrium diagram of the chosen quinary alloy system was calculated using Thermo-Calc software and SGTE binary solution database version 5 and is presented in Fig. 4. The quinary phase diagram shows that above 1200 K, only the BCC_B2 phase is stable, while below 500 K, three HCP and one Laves phase are stable. The liquidus and solidus boundaries of the TiVZrYHf HEA are at temperatures ~1900 K and ~1800 K, respectively. The BCC_B2 phase is the first solid phase that gets precipitated from the liquid phase. At ~1200 K, a disordered HCP_A3 gets precipitated from BCC_B2 which is followed by precipitation of another disordered HCP_A3#2 phase at 1000 K. Due to the diffusive nature of transformation of the BCC_B2 into HCP_A3 and HCP_A3#2, the amount of B2 phase decreased, and the disordered phase increased. At ~ 500 K, all the BCC_B2 transformed into three disordered HCP phases and ZrV_2 (cubic Laves phase). The single-point equilibrium

Table 2
Phase stability parameters calculated using semiempirical approaches, showing phase separation tendency in the quinary alloy system.

ΔH_{mix}(kJ.mol^{-1})	ΔS_{mix}(J.mol^{-1}K^{-1})	$\delta \times 100$(%)	VEC
7	13.38	10.37	4

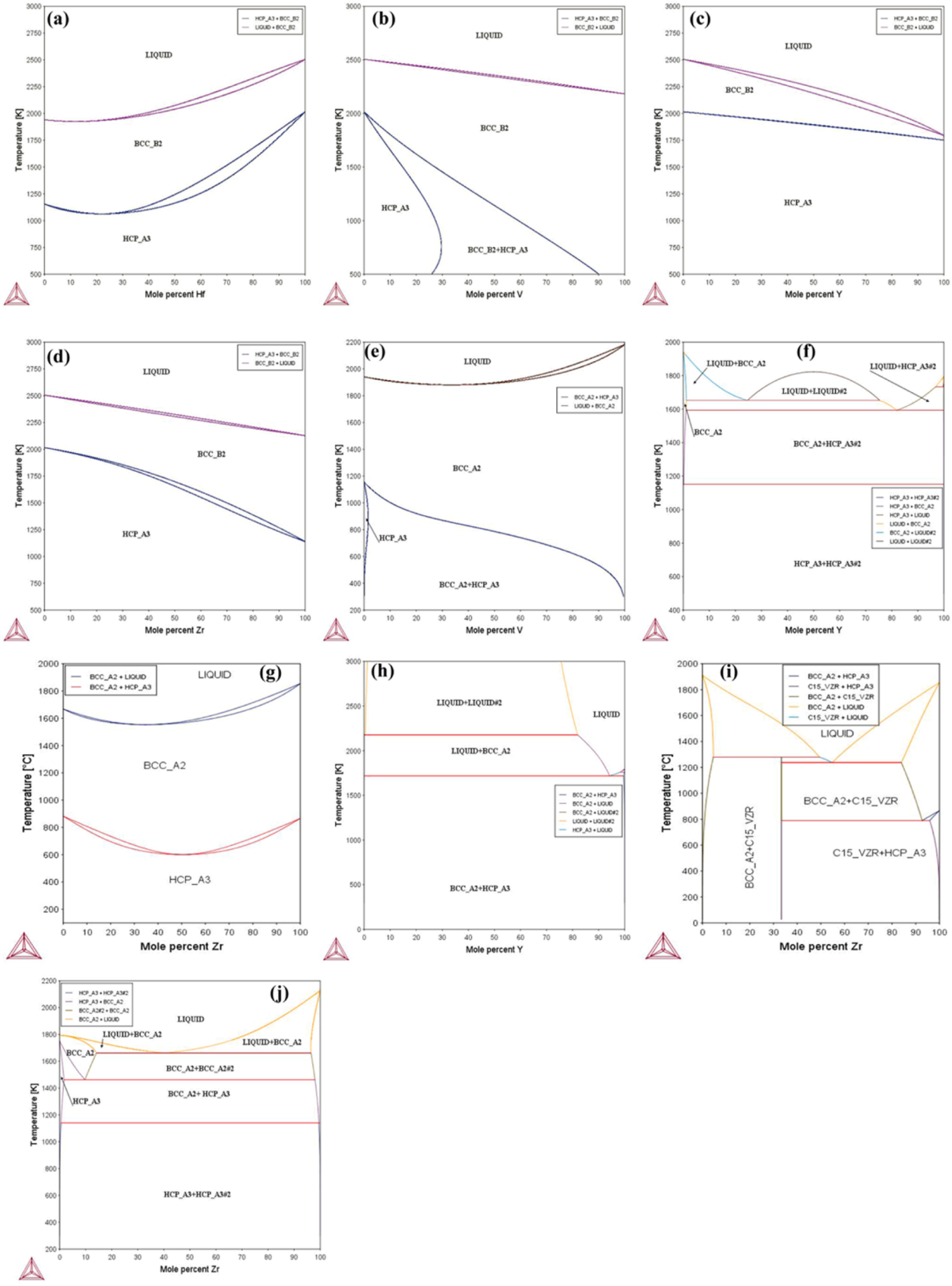

Fig. 3. : Phase diagrams of binary subsystems calculated by Thermo-Calc showing equilibrium phases. The binary phase diagrams are as follows: (a) Hf-Ti (b) Hf-V (c) Hf-Y (d) Hf-Zr (e) Ti-V (f) Ti-Y (g) Ti-Zr (h) V-Y (i) V-Zr (j) Y-Zr.

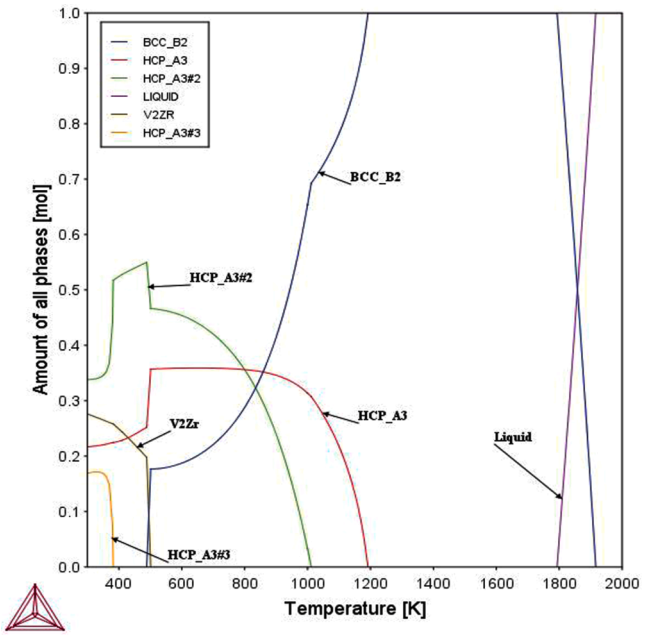

Fig. 4. : Plot of the number of equilibrium phases as a function of temperature in TiVYZrHf RHEA. The phase diagram shows a single BCC_B2 structure above 1200 K and a mixture of three disordered HCP phases and the C15 type Laves phase below 227 K.

calculations done at three temperatures are tabulated in Table 3.

4.2. Phase stability study using DFT

Phase stability of the chosen alloy (TiVZrYHf) was examined using DFT. A 10-atom BCC primitive cell was selected to calculate the minimum energy of formation for the quinary RHEA, as shown in Fig. 1. Similarly, a 10-atom cell of HCP was selected, as shown in Fig. 2. Now the arrangement of the atoms was changed, and the energy of each distinct configuration was calculated. The minimum and the maximum energies of formation are given in Table 4. The critical temperature of the miscibility gap (the consolute point) is calculated by the assuming regular solution model using the formula [37]

$$T_c = \frac{\Omega}{2R} \tag{5.1}$$

where Ω is the interchange energy parameter (in J mol^{-1}), R the gas constant (in J mol^{-1} K^{-1}), and T_c represents the temperature in Kelvin. The formation energy of a few possible intermetallic phases is also calculated and reported in Table 5. The two intermetallics HfV_2 and ZrV_2 were taken from the binary phase diagrams, and the formation energy for these phases was calculated. As Hf and Zr are completely miscible, we also checked the possibility of forming the ternary Laves phase. The formation energies of these ordered phases have only very small differences, showing that the (Hf, Zr)V_2 has minimum energy. Thus, we have considered the formation of the ternary Laves phase in the alloy and indexed it in the XRD pattern.

4.3. Characterization of the annealed sample

The as-cast sample was annealed for 7 h and furnace cooled to ensure formation of equilibrium phases. Then XRD of the annealed sample was done to determine the crystal structure of the phases present, as shown in Fig. 6. From the figure, we can identify three disordered and one ordered phase. The three disordered phases are HCP1 (a = 3.18 ± 0.02 Å, c/a =1.58), HCP2 (a = 3.67 ± 0.02 Å, c/a = 1.55), and BCC (a = 3.16 ± 0.02 Å), while the ordered one is (Hf, Zr)V_2 (C15 type Laves phase, a = 7.41 ± 0.02 Å).

The morphology and microstructure of the annealed sample were examined by SEM, as shown in Fig. 7. From the figure, we can clearly identify three types of microstructures, namely, the major phase marked as 1, the eutectic kind of lamellar phase marked as 2, and the droplet structure (dendrites parallel to the plane of figures) marked as 3. The intergranular boundary of the major phase contains a thin solidified liquid phase marked as 4. To examine the overall composition of the bulk sample full area scan was done to obtain the average composition of the bulk phase, as shown in Fig. 8. All the elements were evenly distributed except Y. The spot analysis of the two varying microstructures was done, as shown in Figs. 9 and 10. Fig. 9 deals with the composition of the primary phase, showing Hf and Zr rich phase with some quantity of Ti alloyed in it. Fig. 10 deals with the lamellar microstructure formed in the alloy, which contains all the elements except Y.

5. Discussion

Parametric calculations were done to understand the initial behaviour of the chosen alloy. The enthalpy of mixing plays an important role in investigating the effect of the thermodynamics on the constituent elements' behaviour in the alloy. The enthalpy of mixing for the binary subsystems was calculated using Miedema's model [31]. The mixing of enthalpy values is tabulated in Table 1. On investigating the values, it can be seen that all the elements have good mutual solubility among themselves except with Y. The V-Zr and Hf-Zr binary systems have significant negative enthalpy values, indicating the chances of forming intermetallic phases. The enthalpy of mixing values of the chosen alloy was calculated using the extrapolation of binary values to a quinary system using a regular solution model [38]. The calculated enthalpy of mixing value (7 $kJ.mol^{-1}$) is shown in Table 2. The atomic size mismatch plays a critical role in the stability of the system. The weighted average of the atomic size mismatch, as tabulated in Table 2, is higher than the desired value, this may destabilise the lattice, and a multiphase microstructure may form. The solid solution forming criteria, as proposed by Zhang et al. [35], was matched with the calculated values of ΔH_{mix}(7 kJ.mol^{-1}), ΔS_{mix}(13.38 J.mol^{-1}.K^{-1}), δ (10.37 %) and VEC (4). In comparison, we found that ΔH_{mix} and δ being out of the given range resulted in the multiphase microstructure.

Examining the binary phase diagrams calculated using Thermo-Calc (Fig. 3) and taken from the Binary Alloy Phase Diagrams book (Fig. 5), we found similar results as predicted by the Miedema method. From phase diagrams, it can be pointed out that Hf-Ti, Ti-Zr, and Hf-Zr show isomorphous phase diagrams, while Hf-V and V-Zr show ordered intermetallics (C15 type Laves phase) at room temperature. The Ti-V phase diagram has some tendency of phase separation. Simultaneously, the binary phase diagrams of the Y with other constituent elements have a high miscibility gap (up to the liquid phase).

The XRD analysis of the annealed sample (Fig. 6) shows four types of phase formation (HCP1, HCP2, BCC1 and C15 Laves phases). The HCP1 (a = 3.18 ± 0.02 Å, c = 5.02 ± 0.02 Å) is the major phase. The SEM-EDS mapping shows that the primary phase is rich in equiatomic type Hf-Zr solid solution with a small amount of Ti. The second type of morphology is shown in Fig. 7, representing a eutectic kind of reaction (lamellar structure). The SEM-EDS compositional analysis illustrates the presence of all elements except Y (Fig. 10). We may predict that the lamellar portion consists of (Hf, Zr)V_2 and Ti-V phase on comparing the XRD and SEM-EDS results. The fourth HCP2 phase is Y rich phase, which solidified, at last forming a droplet-like microstructure as shown in SEM micrographs.

The formation of a multiphase matrix was also supported by DFT calculations shown in Table 4. The critical point of the miscibility gap calculated using DFT calculation and the regular solution model is ~1434 K (1161 °C), while the prediction of CALPHAD shows precipitation of the new phase at ~ 1000 °C. The discrepancies may be due to

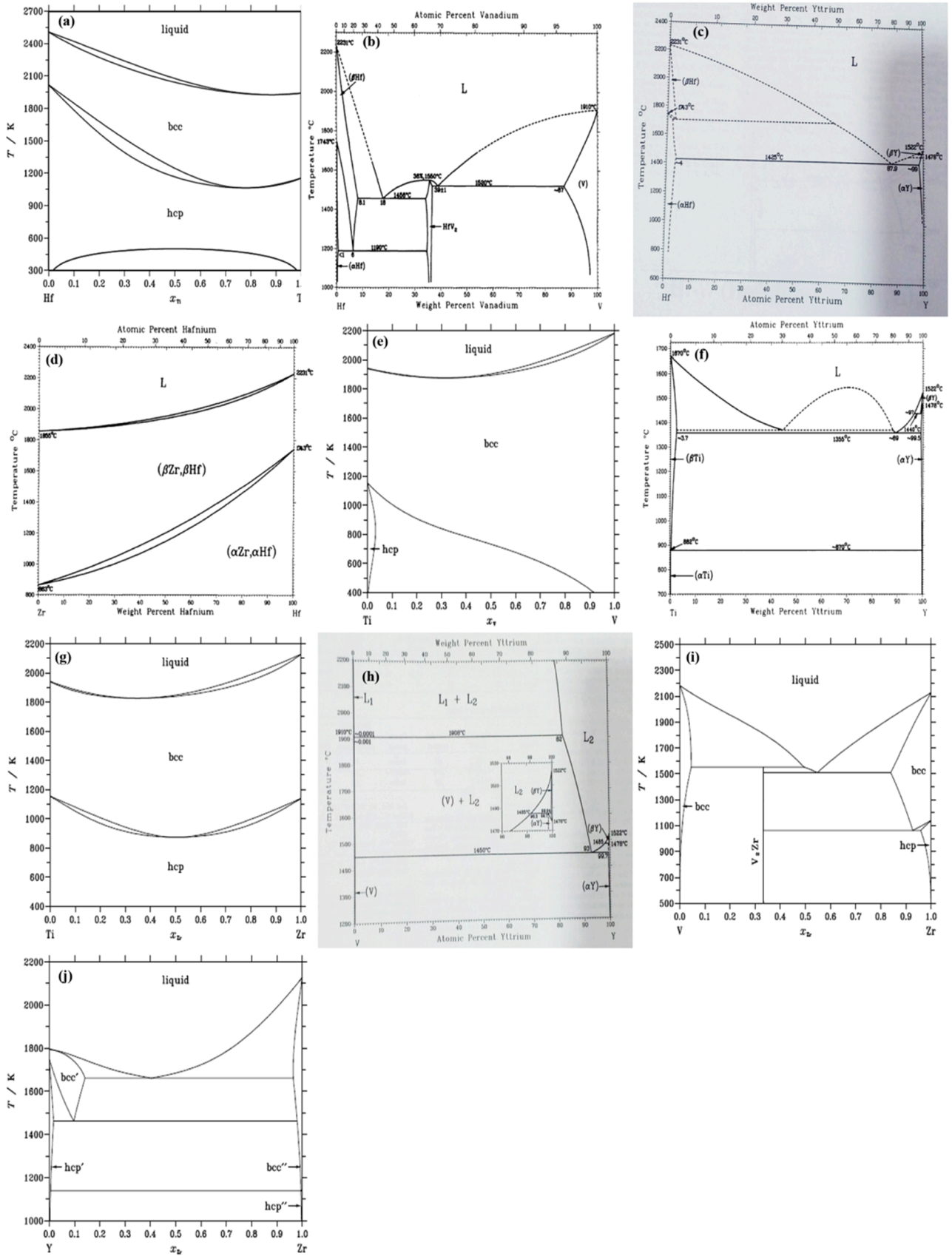

Fig. 5. : Phase diagrams of all the binary subsystems taken from the Binary alloy Phase Diagrams handbook [36] and Landolt-Bornstein database (a) Hf-Ti (b) Hf-V (c) Hf-Y (d) Hf-Zr (e) Ti-V (f) Ti-Y (g) Ti-Zr (h) V-Y (i) V-Zr (j) Y-Zr.

Table 3
Composition of all the phases formed at 300 K, 700 K and 1100 K in mole fraction estimated by single point equilibrium calculation of TiVYZrHf RHEA.

Temp (K)	Equilibrium Phase	Mole fraction	Ti	V	Y	Zr	Hf
300	HCP_A3#1	0.169	0.070	0.080	0.394	0	0.455
	HCP_A3#2	0.217	0.037	0	0	0.498	0.464
	HCP_A3#3	0.338	0.532	0.007	0.395	0	0.066
	C15_ZrV_2	0.276	0	0.667	0	0.333	0
700	HCP_A3#1	0.359	0.203	0.020	0.004	0.540	0.233
	HCP_A3#2	0.420	0.223	0.162	0.372	0.011	0.230
	BCC_B2	0.221	0.151	0.562	0.191	0.006	0.089
1100	BCC_B2	0.782	0.213	0.242	0.248	0.108	0.188
	HCP_A3#1	0.218	0.154	0.047	0.026	0.529	0.243

Table 4
Energy of formation for 10 atoms primitive cell and HCP cell are calculated, and the maximum and minimum values are tabulated. As the formation energy is significantly positive, we have calculated the miscibility gap's critical temperature using a regular solution model.

Phases	BCC		HCP	
	Minimum	Maximum	Minimum	Maximum
TiVYZrHf (kJ.mol^{-1})	30.973	42.380	23.845	39.644
Critical point (K)	1863	2549	1434	2384

Table 5
Formation energy (kJ.mol^{-1}) of possible intermetallics taken from phase diagrams are calculated using DFT.

Phases	HfV_2	ZrV_2	(Hf, Zr)V_2
Formation Energy (kJ.mol^{-1})	−11.897	−10.777	−11.391

Table 6
Prediction of lattice parameter based on the rule of mixture. The lattice parameter of TiZrHf is predicted based on the composition of the major phase obtained from SEM-EDS (Figs. 8, 9 and 10), while that of TiV is assumed to be the equiatomic phase.

Elements	BCC a (Å)	FCC a (Å)	HCP a (Å)	c/a	Lattice parameter (Å) (TiZrHf)	Lattice parameter (Å) (TiV)
Ti	3.24	4.11	2.94	1.58	3.16	3.13
V	3.02	3.81	2.95	1.63		
Y	3.49	5.05	3.65	1.55		
Zr	3.57	4.52	3.23	1.59		
Hf	3.08	4.44	3.19	1.58		

the unavailability of the assessed data of three binary systems (Hf-Y, Ti-Y, and V-Y) in the SSOL5 database of Thermo-Calc software. The strongly positive enthalpy values indicate phase separation and formation of binary and ternary phases. The CALPHAD database used in the present investigation is not updated one. The databases included in Thermo-Calc software are based on the conventional one principal element-based alloy system. Lots of efforts are being made to update these older databases with new strategy of multi-principal alloy systems. We expect that in future DFT assisted modification may be done in the database to increase the accuracy of the phase prediction using CALPHAD for the present alloy system. In the present investigation, CALPHAD software was used to predict the possible phases that may form, and then this was verified by the stability study of those phases using DFT. Thus, the phase stability of binary phases was examined by calculating their formation energy (Table 5). By examining the phase diagrams and the binary enthalpy values we came to know about the possible intermetallic phases that may exist in the present quinary alloy system. However, CALPHAD indicates that binary Laves phase may form in the investigated alloy system, but the Hf and Zr phase diagram analysis developed curiosity to examine the ternary Laves phases also. The calculations indicate the possibility of formation of the ternary

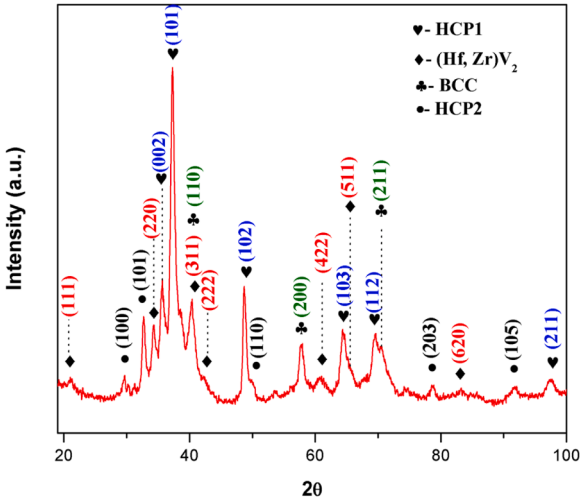

Fig. 6. : Phases evolved after annealing the as-cast sample for 7 h encapsulated in an argon-filled quartz tube at 900 °C.

Laves phase (Cubic type). The lattice parameters of all elements were calculated using DFT (for FCC, BCC and HCP phases). The composition of the primary phase is examined through SEM-EDS (TiZrHf). Applying the rule of mixture using composition from SEM-EDS and the lattice parameter from DFT, the lattice parameter of the TiZrHf disordered phase is predicted to be equal to 3.16 Å. Assuming the BCC phase to be equi-atomic, we have predicted the lattice parameter to be equal to 3.13 Å. The predicted lattice parameters are in accordance with the calculated parameters from XRD.

6. Conclusions

The following conclusions can be drawn from the present work

1. Enthalpy of mixing of TiVYZrHf high entropy alloy was calculated using Miedema model (ΔH_{mix} = 7 kJ.mol^{-1}) found to be close to the proposed range favouring the formation of single-phase solid solution ($-10 \leq \Delta H_{mix} \leq 7kJ.mol^{-1}$). However, the size mismatch factor δ(10.37 %) was on the higher side unfavourable for the formation of the single-phase structures. Similarly, the enthalpy of mixing calculated using DFT (ΔH_{mix}^{DFT} = 23.845 kJ.mol^{-1}) with the minimum value for the HCP phase was obtained.
2. As per the prediction of the CALPHAD approach, three disordered HCP and one Laves phase (ZrV_2) were found to be stable at room temperature, whereas the BCC_B2 phase was identified to be stable above 1000 °C.
3. Annealed samples showed the presence of two disordered HCP1(a = 3.18 ± 0.02 Å, c/a = 1.58) and HCP2 (a = 3.67 ± 0.02 Å, c/a = 1.55), along with BCC (a = 3.16 ± 0.02 Å) and the ordered (Hf, Zr)V_2 phase (C15 type Laves phase, a = 7.41 ± 0.02 Å) supporting the theoretical prediction. The SEM-EDS mapping of the annealed

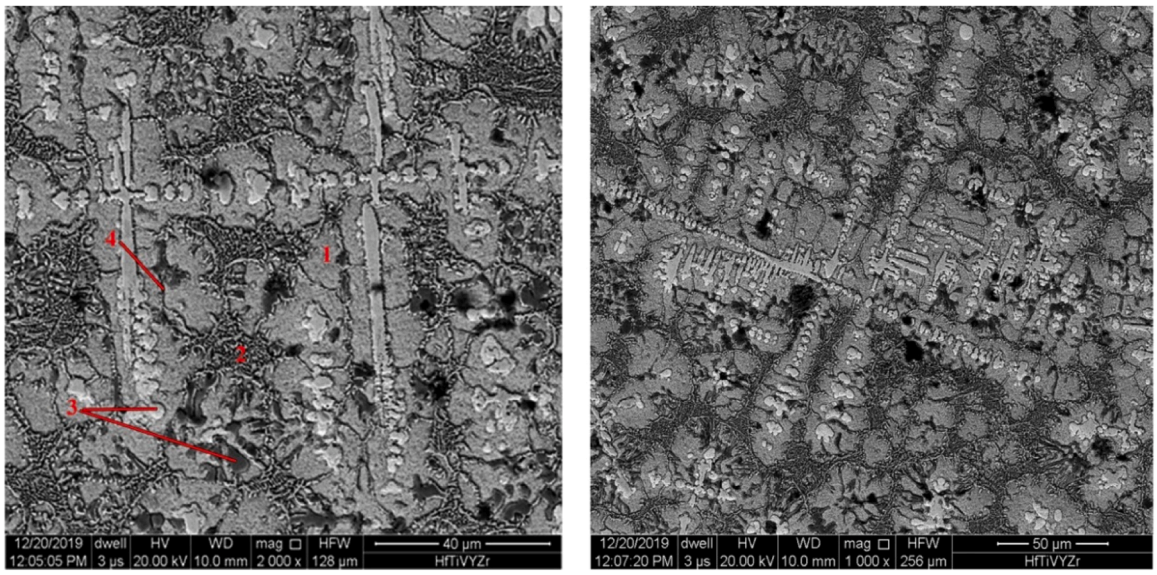

Fig. 7. : SEM micrographs of an annealed sample. The area marked 1 represents the primary phase, while the area marked 2 illustrates the eutectic kind of lamellar phases formed. The area pointed as 3 represents the phase that solidified the last forming droplet kind of structure, while the thin boundary marked as 4 represents the liquid phase between grain boundaries that solidify after the formation of the primary phase.

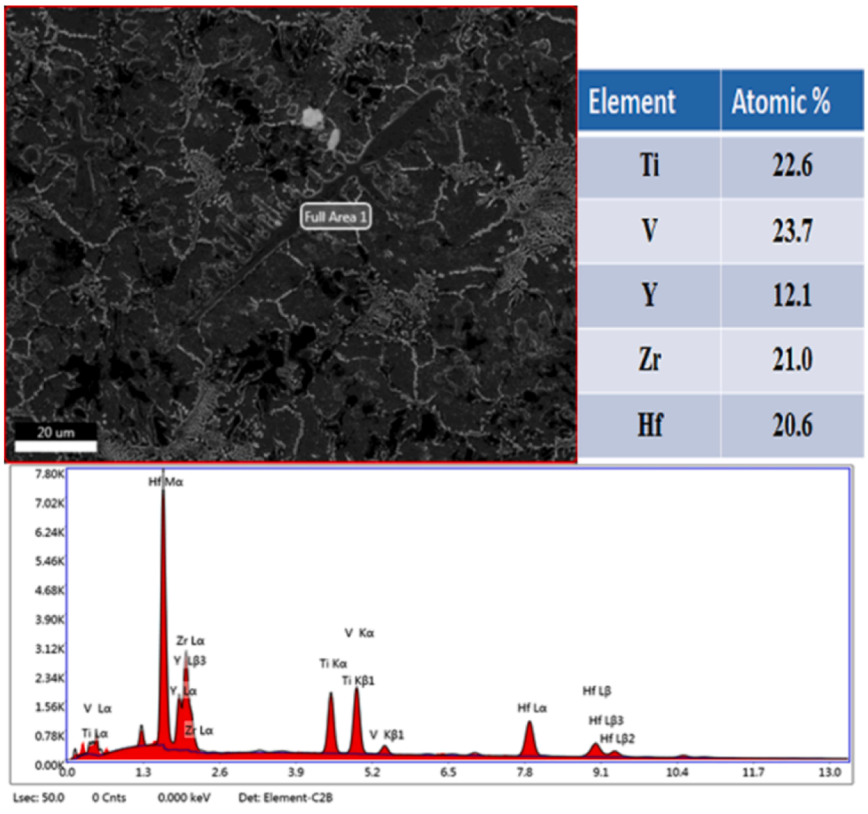

Fig. 8. : SEM-EDAX of the annealed sample. A full area scan is done to obtain the average composition of the bulk sample.

sample revealed that the major phase HCP1 contains predominantly Hf and Zr along with some amount of Ti.

4. Applying the rule of mixture using composition from SEM-EDS and the lattice parameter from DFT, we have predicted the lattice parameter of the TiZrHf disordered phase to be equal to 3.16 Å. Assuming the BCC phase as equi-atomic, we have predicted the lattice parameter to be equal to 3.13 Å. The predicted lattice parameters are in very good agreement with the parameters determined from XRD, namely, 3.18 Å and 3.16 Å, respectively.

CRediT authorship contribution statement

Vivek Kumar Pandey: Writing – original draft, Validation, Methodology, Investigation, Formal analysis, Data curation, Conceptualization. **B. Nageswara Sarma:** Writing – review & editing, Supervision,

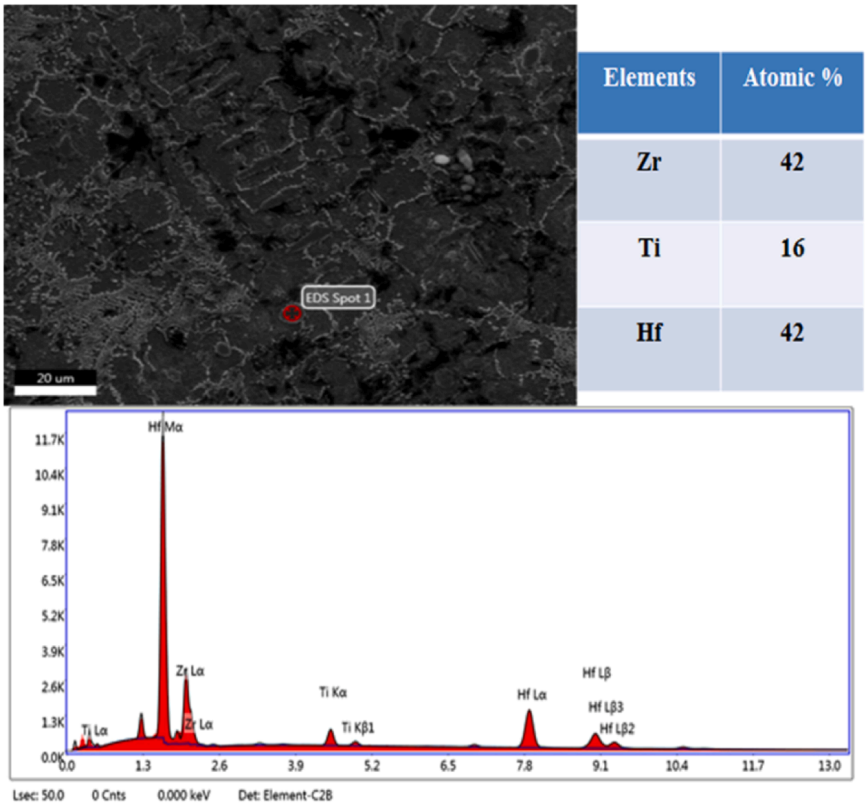

Elements	Atomic %
Zr	42
Ti	16
Hf	42

Fig. 9. : SEM-EDS of the spot on the major phase of the annealed sample.

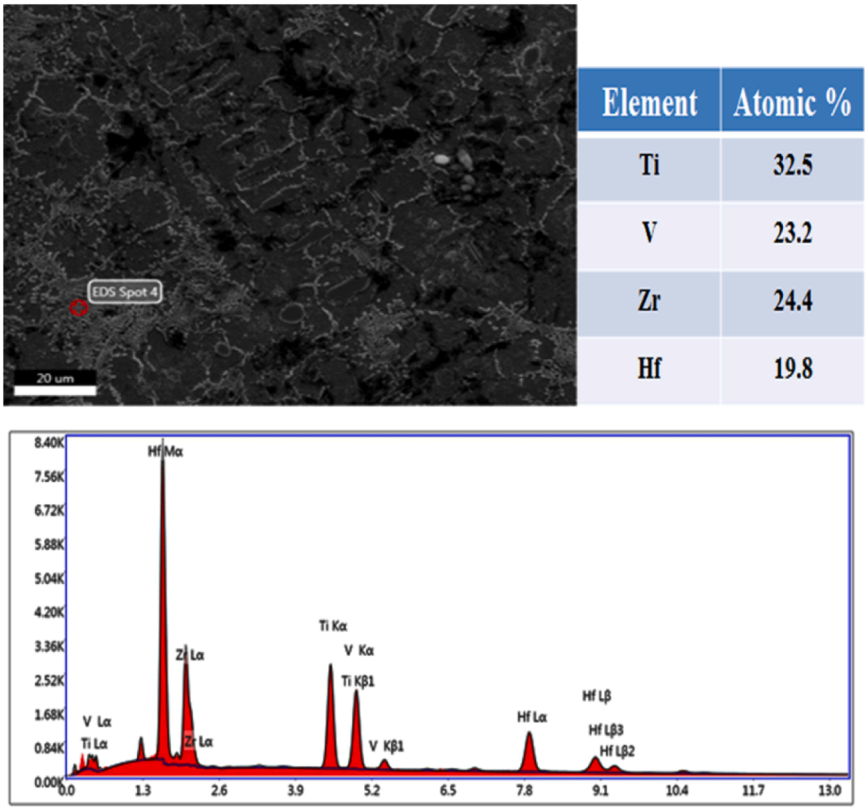

Element	Atomic %
Ti	32.5
V	23.2
Zr	24.4
Hf	19.8

Fig. 10. : SEM-EDS analysis of the lamellar microstructure in the annealed sample showing the presence of all the elements except Y.

Formal analysis, Conceptualization. **N. K. Mukhopadhyay:** Writing – review & editing, Supervision, Formal analysis, Conceptualization.

Declaration of Competing Interest

The authors declare the following financial interests/personal relationships which may be considered as potential competing interests: Vivek Kumar Pandey reports was provided by Indian Institute of Technology (BHU) Varanasi. Vivek Kumar Pandey reports a relationship with Indian Institute of Technology (BHU) Varanasi that includes:. No If there are other authors, they declare that they have no known competing financial interests or personal relationships that could have appeared to influence the work reported in this paper.

Acknowledgement

The authors thank to Dr. S. Lele for continuous discussion on the design and development of BCC and HCP primitive cell for the calculations. The authors also thank Prof. R.K. Mandal and Dr. J. Basu for stimulating discussions. The authors acknowledges help from Dr. R. Manna for extending the facilities of the Advance Research Center for Iron Steel (ARCIS) as its coordinator and Dr. V. Jindal for extending the arc-melting facilities. The authors are also thankful to the Institute's Supercomputing facility (Param Shivay) for running the calculations. The authors would like to thankfully acknowledge the help of Mr. Lalit Kumar Singh and Mr. Girish Sahu in TEM and SEM examination respectively. Support from DST-FIST for TEM investigation is also thankfully acknowledged.

References

[1] J.-W. Yeh, S.-K. Chen, S.-J. Lin, J.-Y. Gan, T.-S. Chin, T.-T. Shun, C.-H. Tsau, S.-Y. Chang, Nanostructured high-entropy alloys with multiple principal elements: novel alloy design concepts and outcomes, Adv. Eng. Mater. 6 (2004) 299–303, https://doi.org/10.1002/adem.200300567.

[2] B. Cantor, I.T.H. Chang, P. Knight, A.J.B. Vincent, Microstructural development in equiatomic multicomponent alloys, Mater. Sci. Eng.: A 375–377 (2004) 213–218, https://doi.org/10.1016/j.msea.2003.10.257.

[3] O.N. Senkov, J.D. Miller, D.B. Miracle, C. Woodward, Accelerated exploration of multi-principal element alloys with solid solution phases, Nat. Commun. 6 (2015) 6529, https://doi.org/10.1038/ncomms7529.

[4] S. Gorsse, D.B. Miracle, O.N. Senkov, Mapping the world of complex concentrated alloys, Acta Mater. 135 (2017) 177–187, https://doi.org/10.1016/j.actamat.2017.06.027.

[5] M. Gao, D. Alman, Searching for next single-phase high-entropy alloy compositions, Entropy 15 (2013) 4504–4519, https://doi.org/10.3390/e15104504.

[6] O.N. Senkov, G.B. Wilks, D.B. Miracle, C.P. Chuang, P.K. Liaw, Refractory high-entropy alloys, Intermetallics 18 (2010) 1758–1765, https://doi.org/10.1016/j.intermet.2010.05.014.

[7] O.N. Senkov, J.M. Scott, S.V. Senkova, D.B. Miracle, C.F. Woodward, Microstructure and room temperature properties of a high-entropy TaNbHfZrTi alloy, J. Alloy. Compd. 509 (2011) 6043–6048, https://doi.org/10.1016/j.jallcom.2011.02.171.

[8] V.K. Pandey, Y. Shadangi, V. Shivam, B.N. Sarma, N.K. Mukhopadhyay, Theoretical and experimental study on phase stability of TiVZrMoW refractory high entropy alloy, Philos. Mag. 102 (2022) 480–503, https://doi.org/10.1080/14786435.2021.2001066.

[9] S. Murty, B.S. Yeh, J.W. Ranganathan, High Entropy Alloys, Butter -Heinemann (2014).

[10] M.C. Gao, J.W. Yeh, P.K. Liaw, High-Entropy Alloys Fundamental and Applications, Springer International Publishing, Cham, 2016, https://doi.org/10.1007/978-3-319-27013-5.

[11] V.K. Pandey, Y. Shadangi, V. Shivam, J. Basu, K. Chattopadhyay, B. Majumdar, B. N. Sarma, N.K. Mukhopadhyay, Synthesis, characterization and thermal stability of nanocrystalline MgAlMnFeCu low-density high-entropy alloy, Trans. Indian Inst. Met. (2020), https://doi.org/10.1007/s12666-020-02114-4.

[12] V. Shivam, J. Basu, V.K. Pandey, Y. Shadangi, N.K. Mukhopadhyay, Alloying behaviour, thermal stability and phase evolution in quinary AlCoCrFeNi high entropy alloy, Adv. Powder Technol. 29 (2018) 2221–2230, https://doi.org/10.1016/j.apt.2018.06.006.

[13] A. Takeuchi, K. Amiya, T. Wada, K. Yubuta, W. Zhang, High-entropy alloys with a hexagonal close-packed structure designed by equi-atomic alloy strategy and binary phase diagrams, JOM 66 (2014) 1984–1992, https://doi.org/10.1007/s11837-014-1085-x.

[14] M. Feuerbacher, M. Heidelmann, C. Thomas, Hexagonal high-entropy alloys, Mater. Res. Lett. 3 (2015) 1–6, https://doi.org/10.1080/21663831.2014.951493.

[15] A. Takeuchi, K. Amiya, T. Wada, K. Yubuta, Dual HCP structures formed in senary ScYLaTiZrHf multi-principal-element alloy, Intermetallics 69 (2016) 103–109, https://doi.org/10.1016/j.intermet.2015.10.022.

[16] L. Rogal, P. Bobrowski, F. Körmann, S. Divinski, F. Stein, B. Grabowski, Computationally-driven engineering of sublattice ordering in a hexagonal AlHfScTiZr high entropy alloy, Sci. Rep. 7 (2017) 2209, https://doi.org/10.1038/s41598-017-02385-w.

[17] T. Nagase, M. Todai, T. Nakano, Development of Ti–Zr–Hf–Y–La high-entropy alloys with dual hexagonal-close-packed structure, Scr. Mater. 186 (2020) 242–246, https://doi.org/10.1016/j.scriptamat.2020.05.033.

[18] É . Fazakas, V. Zadorozhnyy, L.K. Varga, A. Inoue, D.V. Louzguine-Luzgin, F. Tian, L. Vitos, Experimental and theoretical study of Ti20Zr20Hf20Nb20X20 (X=V or Cr) refractory high-entropy alloys, Int. J. Refract. Met. Hard Mater. 47 (2014) 131–138, https://doi.org/10.1016/j.ijrmhm.2014.07.009.

[19] T. Nagase, Y. Iijima, A. Matsugaki, K. Ameyama, T. Nakano, Design and fabrication of Ti–Zr-Hf-Cr-Mo and Ti–Zr-Hf-Co-Cr-Mo high-entropy alloys as metallic biomaterials, Mater. Sci. Eng.: C. 107 (2020) 110322, https://doi.org/10.1016/j.msec.2019.110322.

[20] M. Calin, J. Vishnu, P. Thirathipviwat, M. Popa, M. Krautz, G. Manivasagam, A. Gebert, Tailoring biocompatible Ti-Zr-Nb-Hf-Si metallic glasses based on high-entropy alloys design approach, Mater. Sci. Eng.: C. (2020) 111733, https://doi.org/10.1016/j.msec.2020.111733.

[21] T. Huang, H. Jiang, Y. Lu, T. Wang, T. Li, Effect of Sc and Y addition on the microstructure and properties of HCP-structured high-entropy alloys, Appl. Phys. A 125 (2019) 180, https://doi.org/10.1007/s00339-019-2484-1.

[22] B.L. Gyorffy, Coherent-potential approximation for a nonoverlapping-muffin-tin-potential model of random substitutional alloys, Phys. Rev. B 5 (1972) 2382–2384, https://doi.org/10.1103/PhysRevB.5.2382.

[23] A. Zunger, S.-H. Wei, L.G. Ferreira, J.E. Bernard, Special quasirandom structures, Phys. Rev. Lett. 65 (1990) 353–356, https://doi.org/10.1103/PhysRevLett.65.353.

[24] J.M. Sanchez, F. Ducastelle, D. Gratias, Generalized cluster description of multicomponent systems, Phys. A: Stat. Mech. Its Appl. 128 (1984) 334–350, https://doi.org/10.1016/0378-4371(84)90096-7.

[25] D.De Fontaine, Cluster Approach to Order-Disorder Transformations in Alloys. Solid State Physics, Academic Press, Inc., 1994.

[26] D. Lerch, O. Wieckhorst, G.L.W. Hart, R.W. Forcade, S. Müller, UNCLE: a code for constructing cluster expansions for arbitrary lattices with minimal user-input, Model. Simul. Mater. Sci. Eng. 17 (2009) 055003, https://doi.org/10.1088/0965-0393/17/5/055003.

[27] A. Zunger, First Principals Statistical Mechanics of Semiconductor Alloys and Intermetallic Compounds, in: P.E.A. Turchi, A. Gonis (Eds.), Stalics and Dynamics of Alloy Phose Transformations, Plenum Press, New York, 1994.

[28] A. van de Walle, Multicomponent multisublattice alloys, nonconfigurational entropy and other additions to the Alloy Theoretic Automated Toolkit, Calphad 33 (2009) 266–278, https://doi.org/10.1016/j.calphad.2008.12.005.

[29] A. Seko, Y. Koyama, I. Tanaka, Cluster expansion method for multicomponent systems based on optimal selection of structures for density-functional theory calculations, Phys. Rev. B 80 (2009) 165122, https://doi.org/10.1103/PhysRevB.80.165122.

[30] Y. Mu, H. Liu, Y. Liu, X. Zhang, Y. Jiang, T. Dong, An ab initio and experimental studies of the structure, mechanical parameters and state density on the refractory high-entropy alloy systems, J. Alloy. Compd. 714 (2017) 668–680, https://doi.org/10.1016/j.jallcom.2017.04.237.

[31] A.R. Miedema, P.F. de Châtel, F.R. de Boer, Cohesion in alloys — fundamentals of a semi-empirical model, Phys. B+C. 100 (1980) 1–28, https://doi.org/10.1016/0378-4363(80)90054-6.

[32] A. Takeuchi, K. Amiya, T. Wada, K. Yubuta, W. Zhang, A. Makino, Alloy designs of high-entropy crystalline and bulk glassy alloys by evaluating mixing enthalpy and delta parameter for quinary to decimal equi-atomic alloys, Mater. Trans. 55 (2014) 165–170, https://doi.org/10.2320/matertrans.M2013352.

[33] S. Guo, C. Ng, J. Lu, C.T. Liu, Effect of valence electron concentration on stability of fcc or bcc phase in high entropy alloys, J. Appl. Phys. 109 (2011) 0–5, https://doi.org/10.1063/1.3587228.

[34] S. Fang, X. Xiao, L. Xia, W. Li, Y. Dong, Relationship between the widths of supercooled liquid regions and bond parameters of Mg-based bulk metallic glasses, J. Non-Cryst. Solids 321 (2003) 120–125, https://doi.org/10.1016/S0022-3093(03)00155-8.

[35] Y. Zhang, Y.J. Zhou, J.P. Lin, G.L. Chen, P.K. Liaw, Solid-solution phase formation rules for multi-component alloys, Adv. Eng. Mater. 10 (2008) 534–538, https://doi.org/10.1002/adem.200700240.

[36] H. Okamoto, P.R. Subramanian, L. Kacprzak. Binary Alloy Phase Diagrams, Second, ASM International, 2007.

[37] A. Prince, Alloy Phase Equilibria, Phys. Bull. 17 (1966) 255–256.

[38] U. Thiedemann, M. Rösner-Kuhn, K. Drewes, G. Kuppermann, M.G. Frohberg, Mixing enthalpy measurements of liquid Ti-Zr, Fe-Ti-Zr and Fe-Ni-Zr alloys, Steel Res. 70 (1999) 3–8, https://doi.org/10.1002/srin.199905593.